4. LIQUEFACTION AND LATERAL SPREADING

A distinctive feature of the M_w7.1, 4 September 2010 and the M_w6.2, 22 February 2011 earthquakes was the severity and spatial extent of induced liquefaction in native soils (e.g., Cubrinovski et al., 2011a,b; Green et al, 2012). Figure 4-1 shows the areas that liquefied in both events and the associated fault ruptures. While both earthquakes induced extensive liquefaction, the February event was more devastating to central and eastern Christchurch due to the close proximity of the fault rupture. Immediately after the 22 February 2011 earthquake (i.e., from 23 February to 1 March) an extensive drive-through reconnaissance was conducted to better map the severity of liquefaction in a consistent and systematic manner. The resulting liquefaction documentation map is shown in Figure 4-2. Three areas of different liquefaction severity are indicated: (a) moderate to severe liquefaction (red zones), (b) low to moderate liquefaction (yellow zones), and (c) liquefaction predominantly on roads with some on properties (pink zones). Traces of liquefaction were also observed in other areas. The suburbs to the east of the CBD along the Avon River (Avonside, Dallington, Avondale, Burwood and Bexley) were most severely affected by liquefaction.

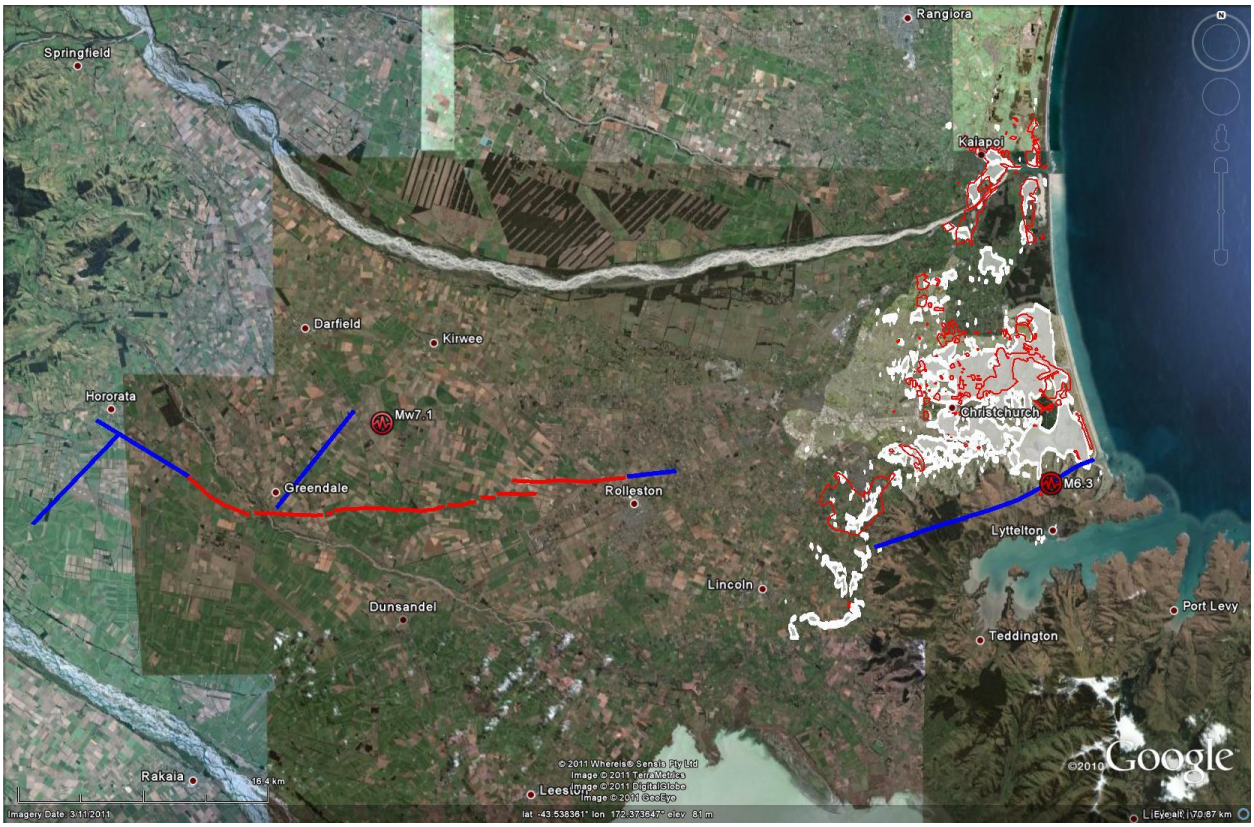

Figure 4-1. Areas of induced liquefaction by the 4 September 2010 (red bordered areas) and 22 February 2011 (white shaded areas) earthquakes and associated fault ruptures (red – fault rupture with surface trace; blue – fault rupture with no surface trace).

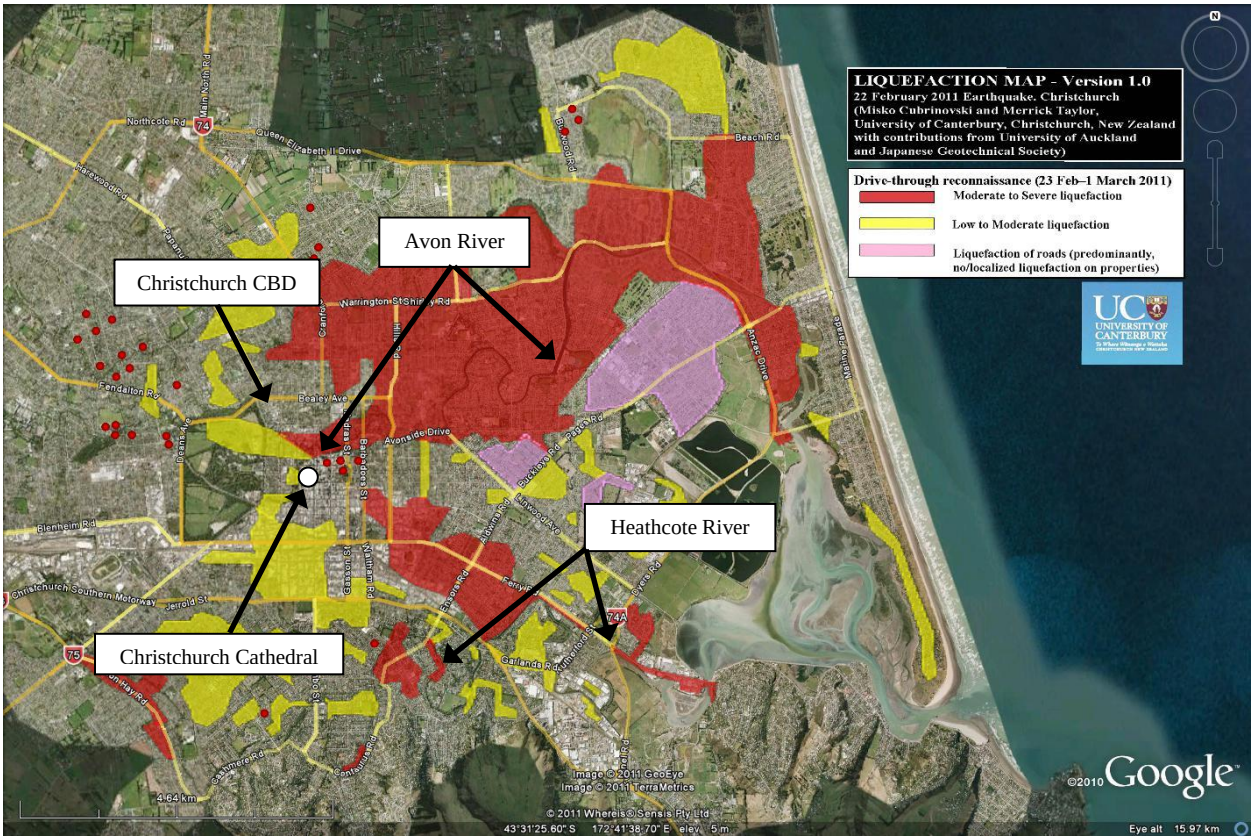

Figure 4-2. Liquefaction documentation map of eastern Christchurch from drive-through reconnaissance.

Brown and Weeber (1992) describe the original site conditions and development of Christchurch as follows: *"Originally the site of Christchurch was mainly swamp lying behind beach dune sand; estuaries and lagoons, and gravel, sand and silt of river channel and flood deposits of the coastal Waimakariri River flood plain. The Waimakariri River regularly flooded Christchurch prior to stopbank construction and river realignment. Since European settlement in the 1850s, extensive drainage and infilling of swamps has been undertaken."* Brown and Weeber also state that surface deposits are actively accumulating and that the present day river channel deposits are excluded from the above-mentioned Christchurch and Springston formations. As a result, the near-surface soils are highly variable. Despite this variability, gross features of the near-surface soil characteristics can be used to explain the performance of observed ground response, particularly in suburban areas. Figure 4-3 provides a schematic illustration of an east-west cross-section of the near surface geology of Christchurch taken along Bealey Avenue (i.e. the center of the city in the East-West direction). As shown it this figure, the water table is only 1 m below the surface in almost the entire eastern side of the city (with the exception of those colluvium areas at the base of the Port Hills to the south). Also, the Riccarton gravel horizon, the upmost aquifer beneath the city, increases with depth going from west to east. Although not shown in Figure 4-

3, it is also noteworthy that the Springston formation (alluvial gravels, sands and silts) is the dominant surface layer in the west of Christchurch, and the Christchurch formation (estuarine, lagoon, beach, dune, and coastal swamp deposits of sand, silt, clay and peat) dominates in the east. Hence, it can be argued that the significant liquefaction observed in the eastern suburbs of the city and the absence in the west of the city can be attributed to several contributing factors: (i) a reduction in the amplitude of ground shaking moving from east to west (Chapter 2); (ii) a gradual change in surficial soil characteristics; and (iii) an increase in water table depth.

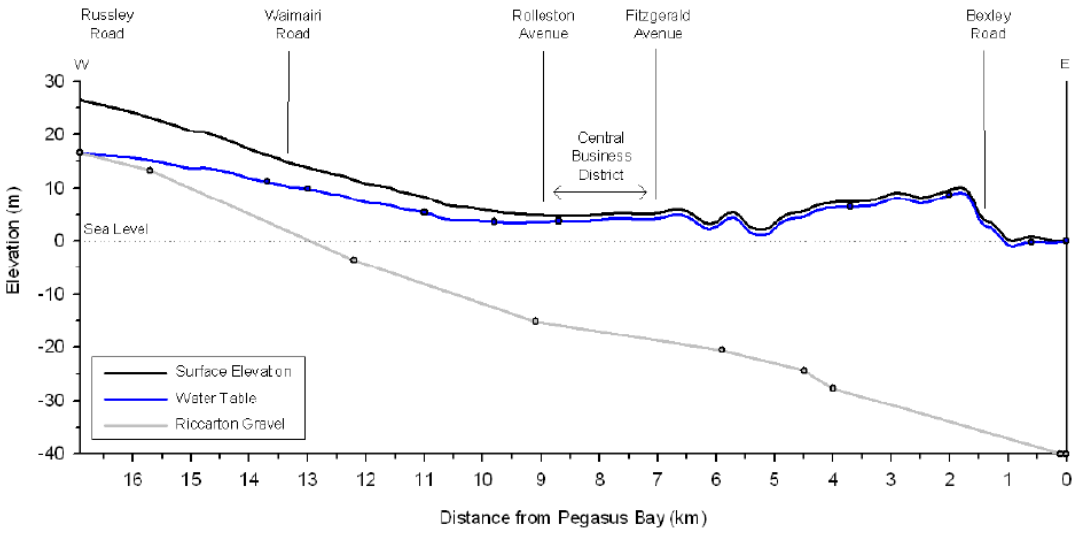

Figure 4-3. East-west cross-section of surface elevation, water table and Riccarton gravel horizon at Bealey Avenue (Cubrinovski and McCahon, 2011).

This chapter is organized into four main sections: Impact of Liquefaction and Lateral Spreading on Residential Areas; Impact of Liquefaction and Lateral Spreading on the Central Business District; Lateral Spreading – Avon River; and In-Situ Test Evaluation of Liquefaction: Observations vs. Predictions.

Impact of Liquefaction and Lateral Spreading on Residential Areas

In both 4 September 2010 and 22 February 2011 earthquakes widespread liquefaction occurred in Christchurch and Kaiapoi causing extensive damage to residential properties. The liquefaction manifested as massive sand boils and large amount of sand/silt ejecta and water littering streets (e.g., Figure 4-4), residential properties, and recreation grounds. Nearly 15,000 residential houses and properties were severely damaged due to liquefaction and lateral spreading, more than half of those beyond an economical repair.

Figure 4-4. Example of severe liquefaction near the intersection of Shortland St and Rowses Rd in the eastern suburb of Aranui. Note the high water marks on the car door window. (-43.521919°, 172.701885°, photo courtesy of Mark Lincoln, nzraw.co.nz)

The distribution of liquefied areas shown in Figures 4-1 and 4-2 reflects the combined effects of the low resistance of the soil to liquefaction (loose cohesionless soil with high water table) and the intensity of the ground motions. The suburbs most severely affected by liquefaction in Christchurch were along the Avon River to the east and northeast of CBD (Avonside, Dallington, Avondale, Burwood, and Bexley). The soils in these suburbs are predominantly loose fluvial deposits of liquefiable clean fine sands and sands with non-plastic silt. The top 5-6 m are in a very loose state, with CPT tip resistances, q_c, of about 2-4 MPa. The resistance typically increases to 7-12 MPa at depths between 6 and 10 m, however lower resistances are often encountered in areas close to wetlands. The more extensive liquefaction observed in these areas during the February 2011 earthquake is consistent with the fact that the seismic loading was about 1.5 to 2.0 times higher during the February event than the September 2010 earthquake. On the contrary however, at the southwest end of the city in Hoon Hay and Halswell, more extensive liquefaction occurred during the 2010 Darfield earthquake due to the more intense shaking experienced in this region during that event.

Examples of damage as a result of liquefaction in the residential areas are presented in Figure 4-5, with the volume of ejected material in residential properties indicated by the piles of sand in Figure 4-5a, a typical view in many streets following the Christchurch earthquake. Figure 4-5b provides a good indication of the flooding and ejected material in the streets themselves immediately following the earthquake. The large sand boils in Figure 4-5c, about 20-30 m long

and 10-15 m wide, indicate both a large severity and extent of liquefaction throughout the depth of the deposit. Figure 4-5d shows typical differential settlement and damage to the building due to separation of walls as a result of loss of bearing capacity of the liquefied foundation materials.

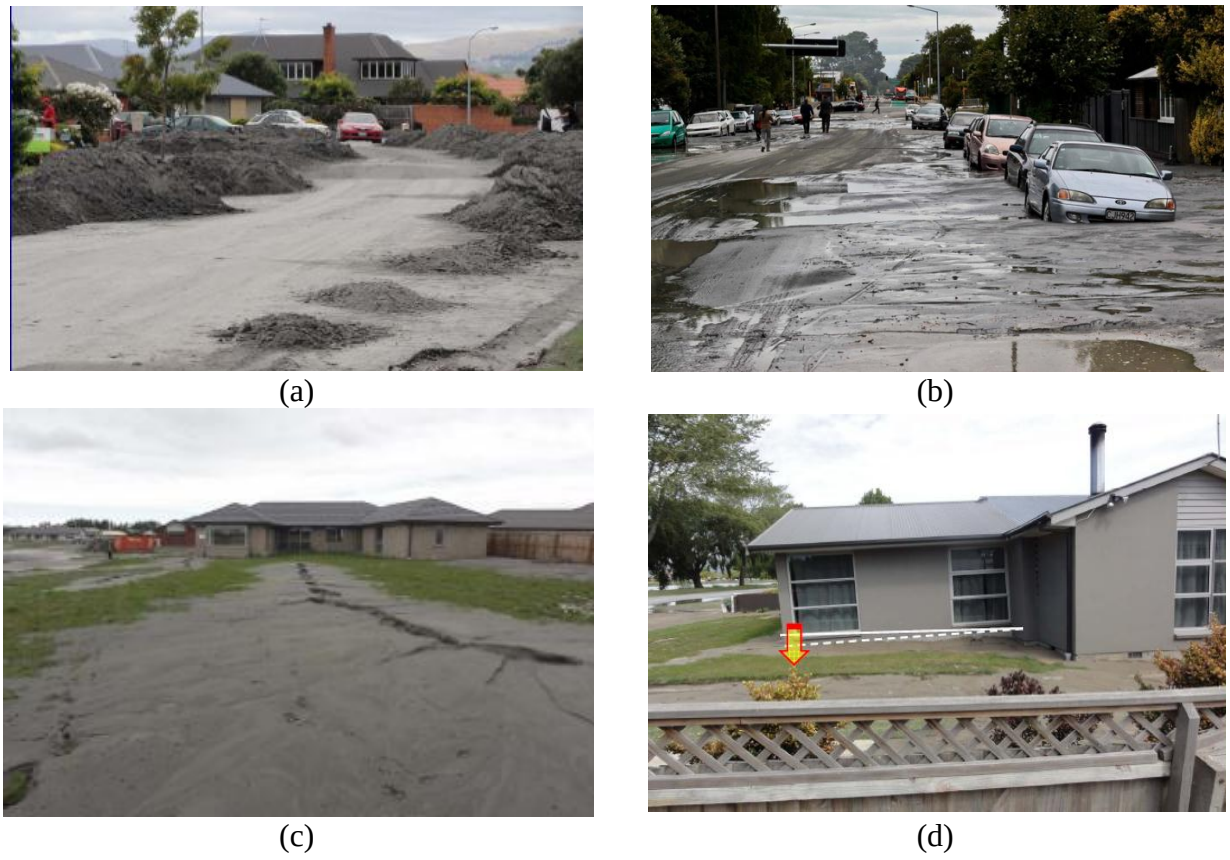

(a) (b)

(c) (d)

Figure 4-5. Typical manifestation of liquefaction in residential areas.

Figure 4-6 shows the damage to a residence in North Kaiapoi after both the Darfield and Christchurch earthquakes. Following the Darfield earthquake there was large settlement of the ground and house, and approximately 40 cm of ejected material covering the ground surface. Site investigations performed following the Darfield earthquake indicated loose/soft soils up to depths of 9 m. Ground motions were largest in Kaiapoi during the Darfield earthquake and lesser in the Christchurch earthquake (PGA's of approximately 0.33 g and 0.21 g, respectively). Despite this, Figure 4-6b shows that the volume of ejected material following the Christchurch earthquake was again significant, and highlights the potential for repeated liquefaction during multiple earthquakes of the typical soil deposits in the region. A smaller volume of ejected material was again evident at this site following the 13 June 2011 earthquakes.

(a) (b)

Figure 4-6. Illustration of a house in North Kaiapoi which sustained liquefaction in both the (a) 4 September 2010 Darfield; and (b) 22 February 2011 Christchurch earthquakes. (-43.38535°, 172.6701°)

Due to the continued threat of the recurrence of liquefaction, the Canterbury Earthquake Recovery Authority (CERA) has divided Christchuch and its environs into four zones: Red, Orange, Green, and White. The zoning was based on observed performance during the earthquake sequence and in-situ geotechnical tests. Detailed information about each of the zones is copied and pasted from the CERA website below. However, in brief, Red Zone = uneconomical to rebuild at this time; Orange Zone = further assessment is required prior to rebuilding; Green Zone = rebuild at will; and White Zone = area not yet assessed. Maps of the zones for Christchurch and Kaiapoi are presented in Figure 4-7. As may be observed from comparing Figures 4-1 and 4-7, there is a close coincidence in the Red Zones marked in Figure 4-7 and areas that are identified in Figure 4-1 as having liquefied during both the Darfield and Christchurch earthquakes. In Christchurch, these areas largely lay along the Avon River and its abandoned channels (i.e., the neighborhoods of Avonside, Dallington, Burwood, Avondale, and Bexley). Additionally, the subdivision of Bexley also is designated as a Red Zone. This subdivision was built on fill and experienced up to 1 m of subsidence during the February earthquake, significantly increasing the flood hazard for the neighbourhood. In Kaiapoi, these areas lay along the Kaiapoi River and Courtenay Stream and their abandoned channels (Wotherspoon et al., 2011).

(a)

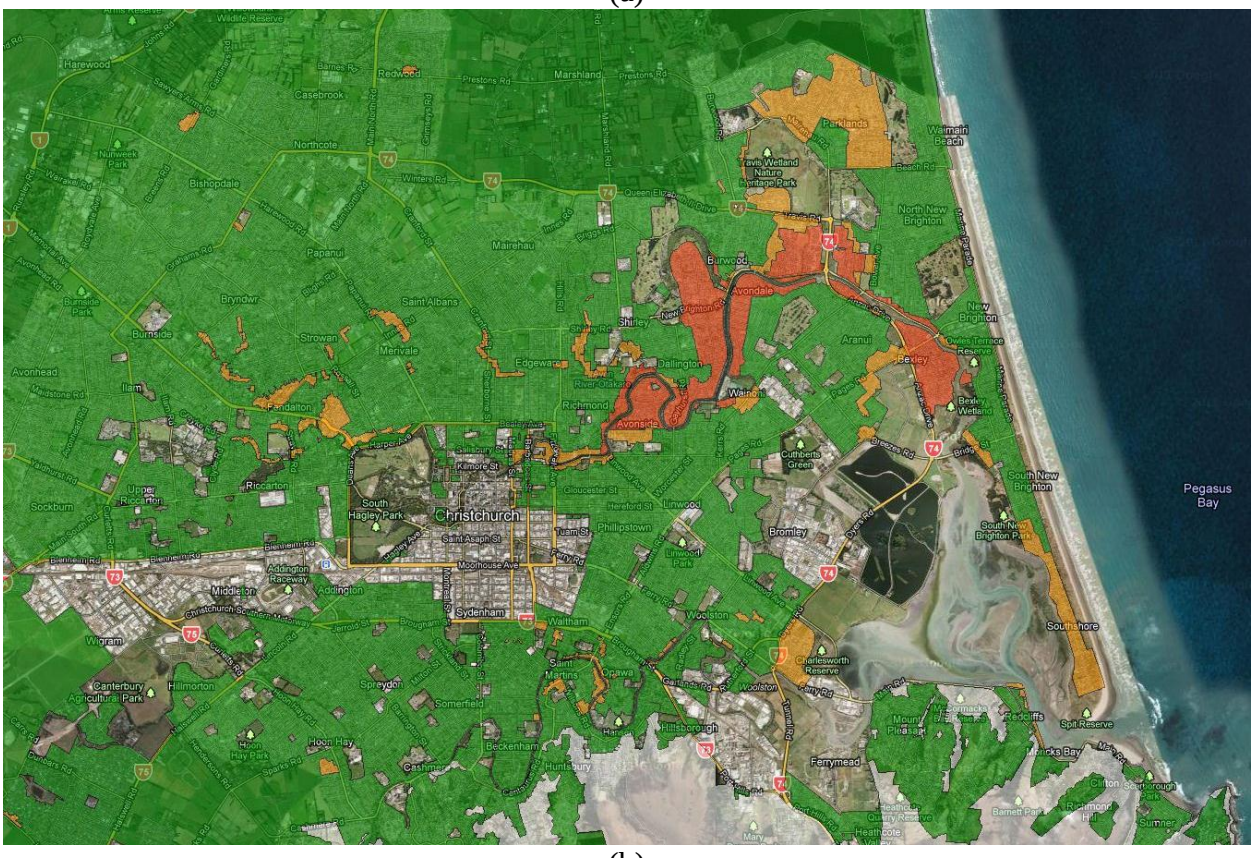

(b)

Figure 4-7. Rebuilding zonation maps: (a) Kaiapoi, and (b) Christchurch. (http://cera.govt.nz/static/land-zone-map/)

Detailed description of the zone classifications copied and pasted from (http://cera.govt.nz/static/land-zone-map/) are given below.

Red Zones: The criteria for defining areas as residential red zone are:

- There is significant and extensive area wide land damage;
- The success of engineering solutions may be uncertain in terms of design, it's success and possible commencement, given the ongoing seismic activity; and
- Any repair would be disruptive and protracted for landowners.

If your property is categorised as red, key points to note are:

- It is not feasible to rebuild on this land at the present time;
- Wide scale land remediation would take a considerable period of time, the social dislocation of such massive works would see homeowners out of their homes for at least three years, and in some cases more than five years;
- In some areas remediation would require up to three metres of compacted fill to bring the land up to compliant height, along with many kilometres of perimeter treatment;
- In addition, a complete replacement of essential infrastructure like sewer, water, electricity and roading would be required;
- Full land repair in these areas may mean that every house would need to be removed, regardless of its degree of present building damage; and
- Even if full land repair was viable, the resulting ongoing social dislocation would have major impacts on schooling, transport and employment for whole communities.

Orange Zones: Land classified as orange means engineers need to undertake further investigation. If your property is classified as orange, key points to note are:

- The orange mapped areas are where engineers need to undertake further investigation;
- Some of the damage in these areas is a direct result of the magnitude 5.6 and 6.3 earthquakes which struck on 13 June, and has not yet been adequately assessed to provide residents with certainty;
- Orange zones will progressively be classified following the outcomes of further investigations.

Green Zones: Land classified as green means that homes are suitable for repair and rebuild. If your property is categorised as green, key points to note are:

- Land generally suitable for houses to be repaired or rebuilt;
- Property owners should talk directly with their insurer or EQC about repairs;
- Property owners no longer have to wait for the results of any area-wide land assessment reports by EQC or their engineering consultants Tonkin & Taylor;

- There will be some isolated exceptions where geotechnical assessments will be required due to major land damage;
- Repair and rebuilding work should take into consideration the risk of ongoing aftershocks, so some finishing tasks such as brick and driveway concrete laying should be delayed until that risk decreases.

White Zone: If your property is classified as white, key points to note are:

- These areas are still being mapped or are not residential;
- In the Port Hills, an extensive geotechnical investigation is underway;
- Land issues – rockfalls – are of a different nature than to those on the plains;
- No timeframes have been set for these areas.

Impact of Liquefaction and Lateral Spreading on the Central Business District

The 22 February 2011 earthquake produced strong ground motions within the central business district (CBD) of Christchurch, which is the central heart of the city just east of Hagley Park and encompasses approximately 200 ha. Some of the recorded ground motions had 5% damped spectral accelerations that surpassed the 475-year return period design motions by a factor of two. Ground shaking caused substantial damage to a large number of buildings. It caused widespread liquefaction and lateral spreading in areas within the CBD, particularly along the stretch of the Avon River that runs through the city. The liquefaction and lateral spreading adversely affected the performance of many multi-storey buildings resulting in global and differential settlements, lateral movement of foundations, tilt of buildings, and bearing failures. The February earthquake was more devastating to the CBD from a geotechnical perspective than the September 2010 earthquake because the latter event did not cause significant liquefaction-within the CBD.

Ten days after the 22 February earthquake, after the urban search and rescue efforts had largely finished, the team initiated a comprehensive ground survey within the CBD to document liquefaction effects in this area. This section of the chapter summarizes the key field observations made by the team.

Christchurch Central Business District

The CBD is the area encompassed by the four avenues, Rolleston to the west, Bealey to the north, Fitzgerald to the east, and Moorhouse to the south. The CBD is relatively densely developed, including multi-storey buildings in its central area, a relatively large number of historic masonry buildings dating from the late 19^{th} and early 20^{th} century, residential buildings (typically two- to five-storey structures located north of Kilmore Street), and some industrial buildings in the south and southeastern part of the CBD. In total, about 3,000 buildings of various heights, age, and structural systems were within the CBD boundaries before the 2010-2011 earthquakes. Latest estimates indicate that about 1,000 of these buildings will have to be

demolished because of excessive earthquake damage. Figure 4-8 outlines the boundaries of the CBD and the approximate surface projection of the causative fault of the 22 February 2011 earthquake.

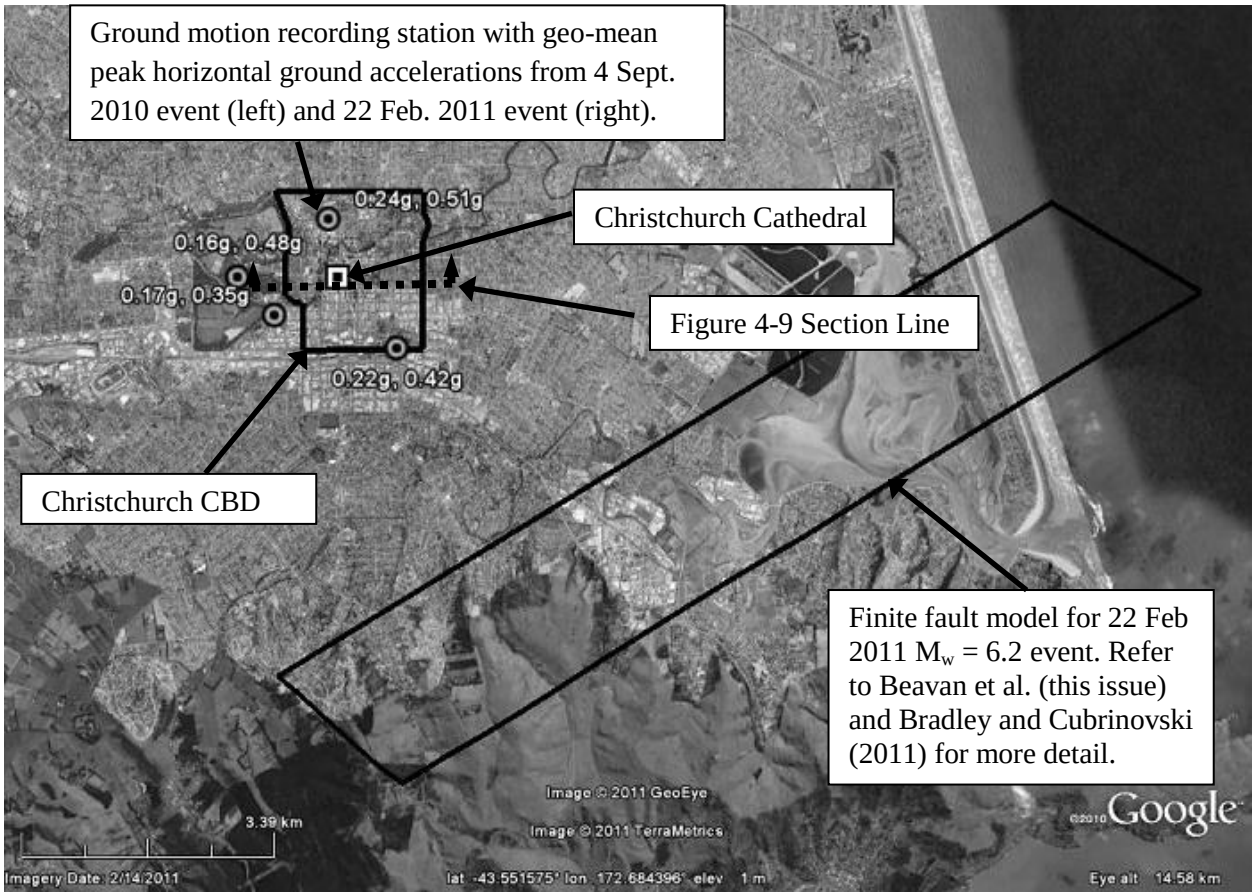

Figure 4-8. Christchurch CBD relative to subsurface fault rupture of 22 February 2011 event.

Site Conditions

Existing geotechnical data indicates different areas within the CBD that are dominated either by gravelly layers, thick liquefiable sands or sandy-silt mixtures, and peat in the top 8-10 m of the deposits. The soil profiles and thicknesses of these layers are highly variable even within a single area. A west to east cross section of the near surface soils in the CBD is shown in Figure 4-9. As may be observed from this figure, the shallow soil deposits (i.e., depths of up to 15-20 m) vary significantly within short distances, both horizontally and vertically. This imposes difficult foundation conditions and sometimes resulted in unconventional or hybrid types of foundations being adopted for buildings. The gravelly soils, even though relatively more competent foundation soils, typically show medium standard penetration test (SPT) N values of about 15 to 25 blow counts, whereas the liquefiable loose sands and silt-sand mixtures have low resistance of

less than N=12 or cone penetration test (CPT) q_c values less than 3-6 MPa. The water table is generally within 1.5 to 2.0 m of the ground surface within the CBD. However, as mentioned above and shown in Figure 4-3, the Riccarton gravel horizon is the upmost aquifer beneath the city, with artesian water pressures, and is at a depth of approximately 22 m below the CBD. This imposed additional restrictions on the use of deep foundations and their associated cost. Additionally, the upward gradient potentially adversely affected the liquefaction resistance of the overlying soils by increasing the pore water pressures in these soils during the 2010-2011 earthquakes.

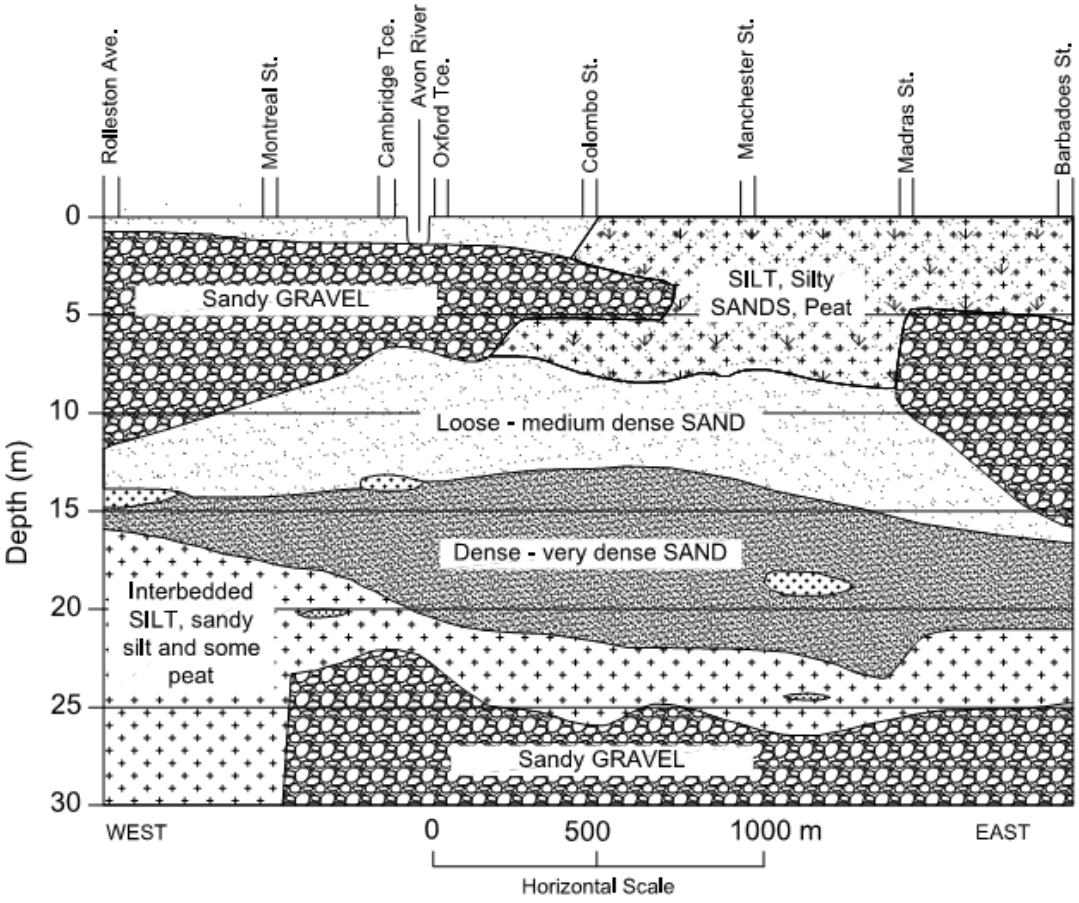

Figure 4-9. Representative subsurface cross section of Christchurch CBD along Hereford Street (reproduced and modified from I. McCahon, personal communication, 19 July, 2011).

Ground Motions and Observed Liquefaction

The M_w7.1, 4 September 2010 Darfield earthquake was caused by a complex rupture of several fault segments, the largest and nearest to Christchurch being on the Greendale fault about 20 km west of the CBD. The maximum horizontal peak ground acceleration (PGA) recorded in the CBD was 0.24 g, with the PGA decreasing generally with distance downstream along the Avon River. The M_w6.2, 22 February 2011 Christchurch earthquake was less than 10 km from the CBD along the southeastern perimeter of the city in the Port Hills (Figures 4-1 and 4-8). The close proximity of this event caused higher intensity shaking in the CBD than the Darfield earthquake. Several of the recordings exhibited significant forward-directivity velocity pulses. In the CBD, horizontal PGAs of between 0.37 g and 0.52 g were recorded. There are four strong motion stations located within or very close to the CBD (Figure 4-8). The recorded PGAs at these four stations are summarized in Table 4-1 for the five earthquakes producing highest accelerations (Bradley and Cubrinovski, 2011).

Table 4-1**.** Geometric mean PGAs and adjusted cyclic stress ratios to M_w7.5 earthquake ($CSR_{7.5}$) for four strong motion stations within/close to CBD, for five earthquakes in the period September 2010 – June 2011

Event	Geometric Mean PGA (g)				Cyclic Stress Ratio $CSR_{7.5}$ [a)]				Magnitude Scaling Factor MSF[b)]
	CBGS	CCCC	CHHC	REHS	CBGS	CCCC	CHHC	REHS	
4 SEP 10 M_w7.1	0.158	0.224	0.173	0.252	0.089	0.127	0.098	0.142	1.15
26 DEC 10 M_w4.8	0.270	0.227	0.162	0.245	0.097	0.082	0.058	0.088	1.80
22 FEB 11 M_w6.3	**0.501**	**0.429**	**0.366**	**0.522**	**0.199**	**0.170**	**0.145**	**0.208**	1.63
13 JUN 11 M_w5.3	0.183	-	0.199	0.188	0.066	-	0.072	0.068	1.80
13 JUN 11 M_w6.0	0.163	-	0.215	0.264	0.060	-	0.079	0.097	1.77

[a)] $CSR_{7.5}$ = 0.65 (PGA/g)/MSF at depth of groundwater

[b)] MSF = $10^{2.24}/M_w^{2.56}$ $\leq$ 1.8 (corresponding to the lower bound range recommended in Youd et al. (2001), with a cap of 1.8)

At shallow depths in the deposits, the variation in the recorded PGA values corresponds closely with variations in the cyclic stress ratio (CSR) for each of these events. Magnitude scaling factors can then be applied to adjust each calculated CSR value to an equivalent value for a M_w7.5 event ($CSR_{M7.5}$) as summarized in Table 4-1 for the geometric mean horizontal values of the PGA (Bradley and Cubrinovski, 2011). The data show that in addition to the high PGAs

during the February earthquake (PGA = 0.37-0.52 g), the CBD buildings were subjected to significant PGAs in the range of 0.16-0.27 g in four additional events. The highest adjusted $CSR_{7.5}$ values of 0.14-0.20 were obtained for the M_w6.2, 22 February 2011 earthquake, which were about 1.6 times the corresponding CSR-values from the M_w7.1, 4 September 2010 Darfield earthquake. Widespread liquefaction occurred only during the 22 February 2011 earthquake in the CBD. Figure 4-10 shows a preliminary liquefaction map for the CBD for the February earthquake (Cubrinovski et al., 2011b).

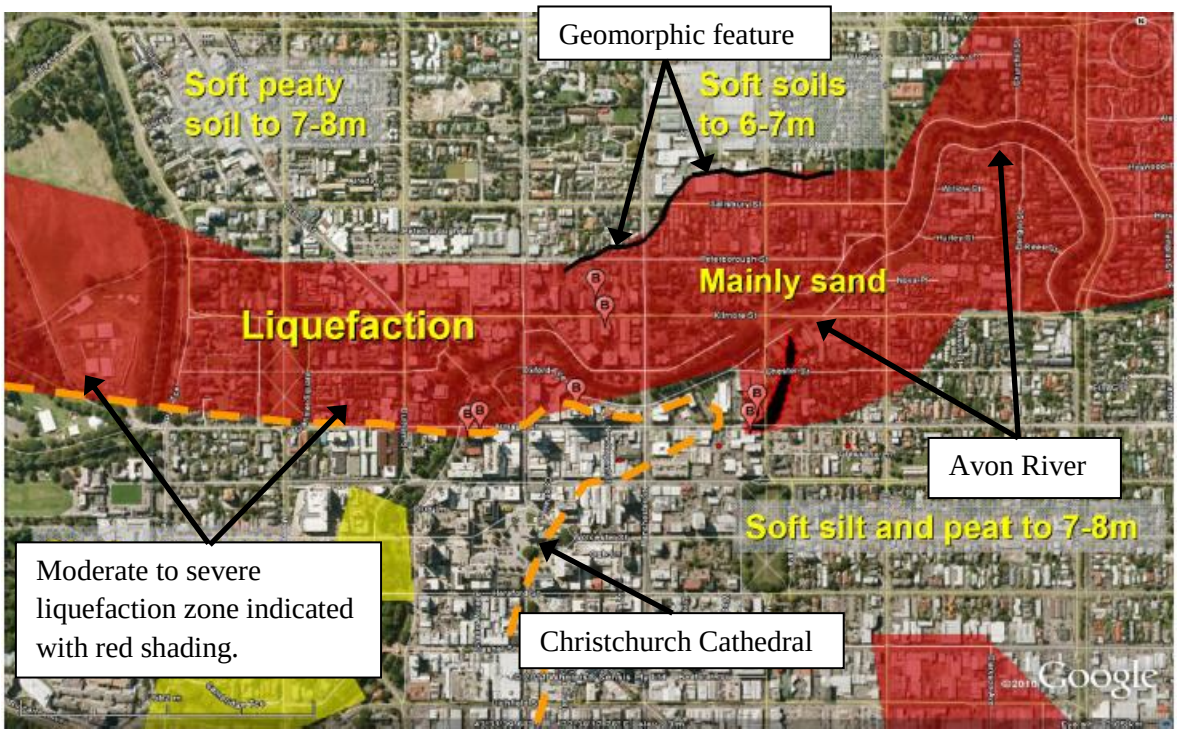

Figure 4-10. Preliminary liquefaction map indicating zones of weakness and locations of buildings discussed in the paper. (Cubrinovski et al., 2011b)

Even though the map shown in Figure 4-10 distinguishes the zone most significantly affected by liquefaction, the severity of liquefaction within this zone was not uniform. The manifestation of liquefaction was primarily of moderate intensity (Figure 4-11a). However, there were also areas of low manifestation or only traces of liquefaction, and also pockets of severe liquefaction with very pronounced ground distortion, fissures, large settlements, and substantial lateral ground movements (Figure 4-11b). This non-uniformity in liquefaction manifestation reflects the complex and highly variable soil conditions even within the CBD principal liquefaction zone. Survey maps of Christchurch dating back to the time of early European settlement (1850's) show a network of streams and swamps scattered across this area (Archives New Zealand, 2011).

(a)

(b)

Figure 4-11. Representative areas of: (a) moderate liquefaction (7 Mar 2011; -43.52791°, 172.63653°), and (b) severe liquefaction within the CBD principal liquefaction zone (4 Mar 2011; -43.52604°, 172.63839°).

The northern extent of the liquefaction zone, which is shown by the black solid line in Figure 4-10, is a clearly defined geomorphic boundary running east-west that was delineated by a slight change in elevation of about 1 m to 1.5 m over an approximately 2 m to 10 m wide zone before the earthquakes. After the February event, it was further characterized by ground fissuring or distortion associated with localized spreading, as well as gentle slumping of the ground surface on the down-slope side. Ground cracks, fissures, and a distorted pavement surface marked this feature, which runs continuously through properties and affected a number of buildings causing cracks in both the foundations and superstructures. Liquefaction and associated ground deformation were pronounced and extensive on the down-slope side between the identified geomorphic feature and the Avon River, but noticeably absent on the slightly higher elevation to the north (upslope side away from the river). This feature is thought to delineate the extent of a geologically recent river meander loop characterized by deposition of loose sand deposits under low velocity conditions. A similar geomorphic feature was observed delineating the boundary between liquefaction damage and unaffected ground within a current meander loop of the river to the east of this area (Oxford Terrace between Barbadoes Street and Fitzgerald Avenue).

Impact of Liquefaction and/or Lateral Spreading on Structures

Described below are select cases where structures were impacted by liquefaction and/or lateral spreading.

1. Ground Failure Effects on Nearly Identical Structures – East Salisbury Area

A mini-complex of three nearly identical buildings (with one small but important difference) is shown in Figure 4-12. The buildings are three-storey structures with a garage at the ground floor, constructed on shallow foundations. This case clearly illustrates the impact of liquefaction, as the

nearly identical structures have been built across the east-west trending geomorphic feature identified previously in Figure 4-10, with one building located on the higher level to the north suffering no damage, and the buildings located below the crest suffering progressively higher amounts of damage. This geomorphic feature, which is expressed here by a significant change in grade of the pavement between the northern and middle buildings, is shown in Figure 4-13. The northern building that sits on the higher ground showed no evidence of cracking and distortion of the pavement surface. Conversely, large sediment ejecta were found along the perimeter of the southern building indicating severe liquefaction in its foundation soils (Figure 4-12b). Liquefaction features were also observed near the middle building, but the resulting distress of this building was significantly less than that of the southern building. The southern building had a shortened end wall with a column at its southwest corner, which appeared to have experienced additional settlement at the location of the column's concentrated load. The building suffered differential settlement of about 40 cm and more than 3 degrees of tilt towards the west-southwest, which is visible in Figure 4-12a.

(a) (b)

Figure 4-12. Apartment complex: (a) looking south from northern building showing tilt of southern building, and (b) looking north at liquefaction feature at edge of southern building (7 Mar 2011; -43.52434°, 172.64432°).

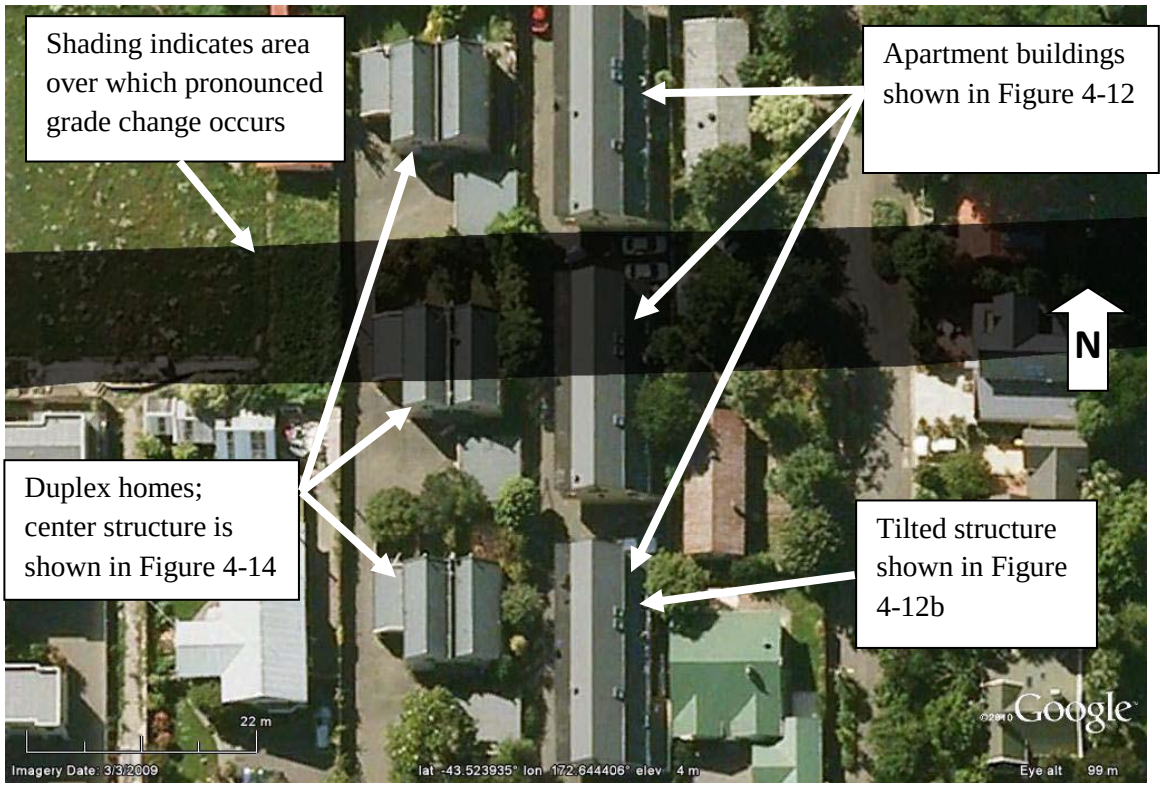

Figure 4-13. Location of geomorphic feature in area of apartment and duplex complexes north of Salisbury Street in CBD.

Adjacent to these buildings is another complex of three identical buildings, which are structurally different buildings from the former set. Their locations relative to the abovementioned geomorphic feature is identical, but these buildings are two-storey duplexes that are apparently supported on different foundations. Figure 4-14a shows the middle building with clear evidence of pavement distortion, cracking and settlement of the surrounding ground. The settlement of the building was likely not significant, but the ground settled about 20 cm exposing the top of the foundation at the southwest corner (Figure 4-14b).

Another apartment complex, constructed on a single level basement that extends almost the full length of the complex and provides off-street parking for the development, lies to the west of the two case histories discussed previously. It also crosses the geomorphic feature. Noticeable settlement of the ground at the southern end of the complex of the order of 15-20 cm occurred and compression features in the pavement suggest that it displaced laterally toward the street. The concrete basement floor and structure appeared to have undergone negligible distortion, which indicates an overall rigid response despite the differential ground movements across the site.

(a) (b)

Figure 4-14. Duplex housing complex: (a) looking north at center building, and (b) close-up of ground settlement next to center building (16 Mar 2011; -43.52399°, 172.64417°).

2. Punching Settlement - Madras-Salisbury-Peterborough Area

Several buildings with shallow foundations located within the liquefied zone underwent punching settlements with some undergoing significant differential settlements and bearing capacity failures. An example of such performance is shown in Figure 4-15 for a two-storey industrial building located 200 m south-west of the buildings discussed previously. There are clear marks of the mud-water ejecta on the walls of the building indicating about 25-cm-thick layer of water and ejected soils due to the severe liquefaction. Note the continuous sand ejecta around the perimeter of the footing and signs of punching shear failure mechanism in Figure 4-15. At the front entrance of the building large ground distortion and sinkholes were created due to excessive pore water pressure and upward flow of water. Settlement of the building around its perimeter was evident and appeared substantially larger than that of the surrounding soil that was unaffected by the building. The building settled approximately 25 cm relative to a fence at its southeast corner and settled 10-20 cm relative to the ground at its northwest corner. The ground floor at the entrance was uplifted and blistered which is consistent with the pronounced settlement beneath the walls along the perimeter of the building.

Figure 4-15. Two-story building that underwent liquefaction-induced punching movements (7 Mar 2011; -43.52506°, 172.64176°).

3. Differential Settlement and Sliding - Armagh-Madras Area

Farther to the south, at the intersection of Madras and Armagh Streets, several buildings were affected by severe liquefaction that induced significant differential settlements or lateral movements. At this location, the liquefaction was manifested by a well-defined, narrow zone of surface cracks, fissures, and depression of the ground surface about 50 m wide, as well as water and sand ejecta (Figure 4-16). This zone stretches from the Avon River to the north toward the buildings affected by this liquefaction feature, shown in the background of Figure 4-16, to the south. Traces of liquefaction were evident further to the south of these buildings.

The building shown in Figure 4-17 is a three-storey structure on shallow foundations that settled substantially at its front, resulting in large differential settlements that tilted the building about 2 degrees. The building was also uniformly displaced laterally approximately 15 cm toward the area of significant liquefaction near the front of the building (i.e., to the north). There was a large volume of sand ejecta at the front part of the building with ground tension cracks propagating east of the building and in the rear car-park that are consistent with the lateral movement of the building toward the north.

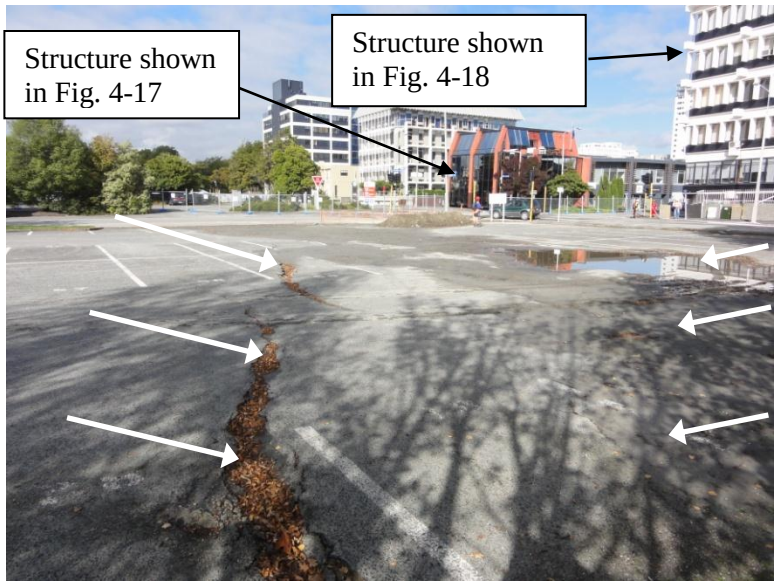

Figure 4-16. Relatively narrow liquefaction-induced feature that traverses parking lot northeast of the intersection of Madras and Armagh streets (24 Mar 2011; -43.52842°, 172.64308°).

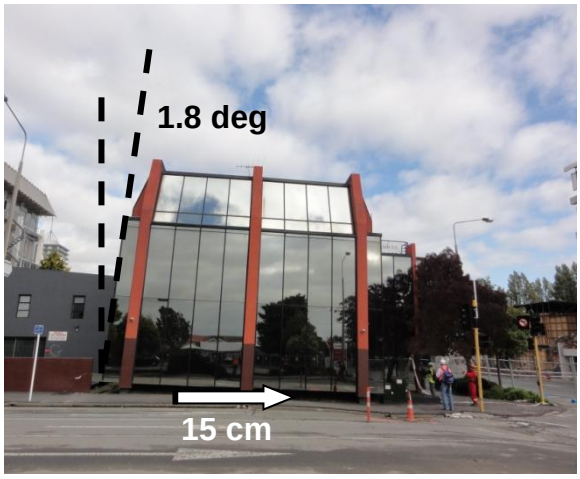

(a)

(b)

Figure 4-17. Liquefaction-induced differential settlement and sliding of building in the CBD (24 Mar 2011; -43.52878°, 172.64252°).

The building shown in Figure 4-18 is immediately across the street to the north. It is a six-storey building on isolated footings with tie beams and perimeter grade beam. The isolated footings are 2.4 m x 2.4 m and 0.6 m deep. Figure 4-18 shows the view of the building looking toward the west and indicates total settlements measured relative to the building to its north, which did not appear to settle. Starting from its northern edge and proceeding south, the differential settlement is 1 cm for the first span, 1 cm for the second span, then 3 cm, 9 cm, and 11 cm, respectively, for

the final three spans. This results in an overall differential settlement across the structure of 25 cm, with 20 cm of it occurring across the two southernmost spans. A strong tie beam that was 0.6 m wide and 1.2 m deep was used between the footings for the first two northernmost spans, whereas the tie beams between the footings for the remaining spans were only 0.3 m wide and x 0.45 m deep. This foundation detail, together with the fact that the observations of liquefaction were most severe at the southeast corner of the building and diminished across the footprint of the building toward the north, led to substantial differential settlements and pronounced structural distortion and cracking. Both buildings were considered uneconomical to repair and were demolished after the February earthquake.

(a) (b)

Figure 4-18. Building undergoing significant liquefaction-induced differential settlement due to part of it being founded on the liquefaction feature in this area (24 Mar 2011; -43.52878°, 172.64252°).

4. Performance of Adjacent Structures - Town Hall Area

The Christchurch Town Hall for Performing Arts, designed by Sir Miles Warren and Maurice Mahoney and opened in 1972, is located within the northwest quadrant of the CBD, with the meandering Avon River to its immediate south. It is a complex facility comprising a main auditorium (seating 2,500) with adjoining entrance lobby, ticketing, and café areas. Further extensions provide a second, smaller auditorium, the James Hay Theatre (seating 1,000), and a variety of function rooms and a restaurant. The structures are supported on shallow foundations except the kitchen facility, which was added later. Air bridges connect the complex to the Crowne Plaza, a major hotel, and to the Christchurch Convention Centre (opened 1997) to the north. Tiled paved steps lead from the southern side of the complex down to the river's edge, with fountains and views across to Victoria Park.

The facility suffered extensive damage caused primarily by liquefaction-induced ground failure. Differential settlements, caused by punching shear beneath the building's main internal columns

that surround the auditorium and carry the largest dead loads to shallow foundations and a second ring of exterior columns (Figure 4-19a) that are connected to the inner ring via beams (Figure 4-19b), caused distortion to the structure. The cracked beam shown in Figure 4-19b underwent an angular distortion of 1/70 across its span. The seating for the auditorium has been tilted and dragged backwards due to the settlement of the surrounding columns. Additionally, the floor of the auditorium is now domed due to differential uplift relative to the columns. The air bridge connecting the main auditorium to the Christchurch Convention Centre to the north (away from river) has separated from the building. With no significant deformations of the ground as the obvious source of this lengthening between the two buildings, the explanation appears to be that distortions to the auditorium structure have pulled the outer walls in toward the building, creating this separation. The entire complex appears to have moved laterally toward the river (albeit by a barely perceptible amount on the northern side) with parts of the complex closest to the river undergoing increasingly larger movements (Figure 4-19c). These sections have settled and moved laterally toward the river more than the remainder of the building, leading to significant structural deformations where the extension and original structures are joined.

(a) (b) (c)

Figure 4-19. Town Hall auditorium and adjacent dining facility undergoing significant liquefaction-induced differential settlement and lateral movements (24 Mar 2011; -43.52727°, 172.63521°).

Contrary to the liquefaction-induced punching settlement of buildings into the surrounding ground that was observed at the Town Hall and in other parts of the CBD, the seven-storey building shown in Figure 4-20a did not punch significantly into the liquefied ground nor undergo significant differential settlement. As shown in Figure 4-20b there were significant amounts of sand ejecta observed in this area. However, there was no obvious evidence of significant differential ground or building movement (Figure 4-20c). The differential settlement measured between adjacent columns was typically negligible, but differential settlements of up to 3.5 cm were measured at a few locations. This building is across the street and slightly to the west of the Town Hall. It is a case of liquefaction without significant differential settlement and building damage.



(a) (b) (c)

Figure 4-20. Building in area of significant liquefaction that displays negligible to minor differential settlement or punching settlement (24 Mar 2011; -43.526508°, 172.634646°).

5. Contrasting Performance of a Pile-Supported Structure - Kilmore Area

Several pile-supported structures were identified in areas of severe liquefaction. Although significant ground failure occurred and the ground surrounding the structures settled, the buildings supported on piles typically suffered less damage. However, there are cases where pile-supported structures were damaged in areas that underwent lateral spreading near the Avon River. In other cases, such as the building shown in Figure 4-21, which is located approximately 200 m to the east from the Town Hall, the ground-floor garage pavement was heavily damaged in combination with surrounding ground deformation and disruption of buried utilities. The settlement of the surrounding soils was substantial, with about 30 cm of ground settlement on the north side of the building and up to 17 cm on its south side. The first-storey structural frame of the building that was supported by the pile foundation with strong tie-beams did not show significant damage from these liquefaction-induced ground settlements.

Across from this building to the north is a seven-storey reinforced concrete building on shallow spread footing foundations that suffered damage to the columns at the ground level. This building tilted toward the southeast as a result of approximately 10 cm differential settlement caused by the more severe and extensive liquefaction at the south-southeast part of the site. It is interesting to note that in the vicinity of this building, the site contained areas that liquefied during the 4 September 2010 earthquake. Following the extensive liquefaction in the 22 February 2011 event, there was also significant liquefaction in some areas during the 13 June 2011 earthquakes.

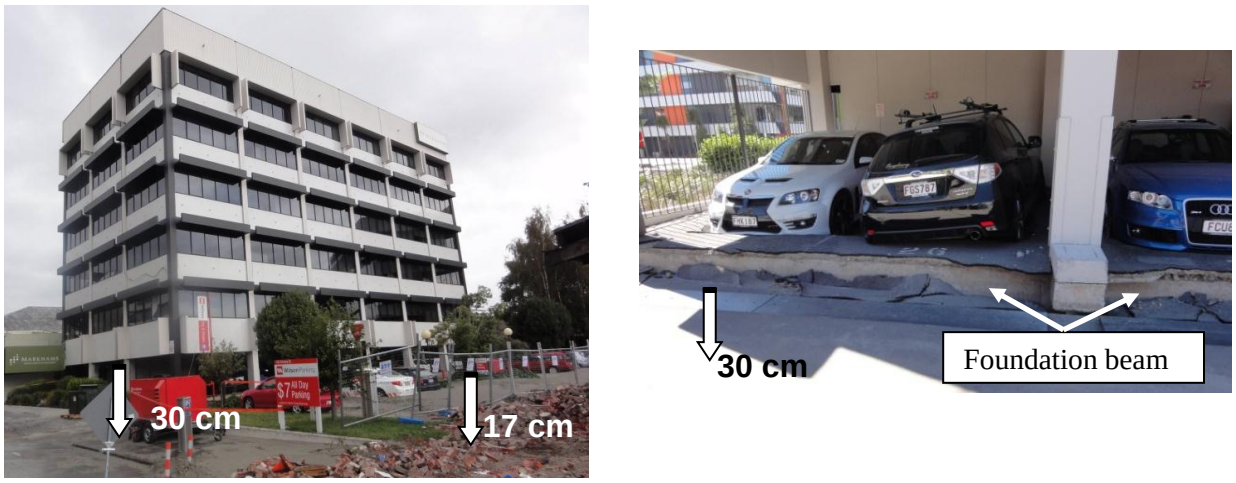

(a) (b)

Figure 4-21. Building on pile foundations in area of severe liquefaction showing large settlement of the surrounding soils relative to the foundation beams (4-6 Mar 2011; -43.526575°, 172.638668°).

6. Presence of Shallow Gravelly Soils - Victoria Square

Near Victoria Square, the liquefied zone was composed predominantly of relatively deep loose sand deposits that transitioned relatively sharply into a zone where gravelly soil layers reach close to the ground surface. Shallow foundations (spread footings and rafts) for many of the high-rise buildings in this latter area are supported on these competent gravelly soils. However, the ground conditions are quite complex in the transition zone, which resulted in permanent lateral movements, settlements, and tilt of buildings either on shallow foundations or hybrid foundation systems, as illustrated in Figure 4-22. Immediately to the north of these buildings, the liquefaction was severe with massive sand ejecta; however, approximately 100 m and further to the south where the gravels predominate, there was neither evidence of liquefaction on the ground surface nor visible distress of the pavement surface. Again, it appears that the ground and foundation conditions have played a key role in the performance of these buildings, which therefore have been selected for in-depth field investigations.

Figure 4-22. Buildings on shallow and hybrid foundations in transition area from moderate liquefaction to low/no liquefaction; arrows indicate direction of tilt of the buildings (7 Mar 2011; -43.52878°, 172.63528°).

Lateral Spreading – Avon River

Along the Avon River, particularly to the east of CBD, lateral spreading occurred, causing horizontal displacements at the river bank on the order of several tens of centimeters to more than two meters. At ten locations along the Avon River, where lateral spreading measurements were conducted after the September 2010 earthquake, measurements of lateral spreading displacements were carried out again after the February earthquake. It was found that the permanent lateral displacements were two to three times the displacement measured after the September earthquake, indicating increased spreading movement which is in agreement with the more severe liquefaction observed in these areas during the February event. Ground surveying indicated that ground cracks associated with lateral spreading extended as far as 100-200 meters from the river, while other aerial observation methods suggest that the effects of spreading might have been even beyond these distances. An example of lateral spreading along the Avon River is shown in Figure 4-23.

Figure 4-23. Example of lateral spreading along the Avon River.

In-Situ Test Evaluation of Liquefaction: Observations vs. Predictions

Following both the Darfield and Christchurch earthquakes, team members performed in-situ tests using the DCP and SASW (Green et al., 2011b). Both tests are portable and provide information about the subsurface properties, making them suitable for immediate post-earthquake reconnaissance investigations. Of particular interest to the team were the properties of the soils that liquefied in either, or both, the Darfield and Christchurch earthquakes. In the following, the DCP and SASW equipment, tests performed, and data reduction are described in more detail.

Dynamic Cone Penetrometer (DCP)

The dynamic cone penetrometer (DCP) used for this reconnaissance was designed by Professor George Sowers (Sowers and Hedges, 1966) and is shown in Figure 4-24. This system utilizes a 6.8 kg mass (15-lb drop weight) on an E-rod slide drive to penetrate an oversized 45° apex angle cone. The cone is oversized to reduce rod friction behind the tip. At sites that liquefied, the DCP tests were performed in hand-augered holes that were bored to the top of the layer that liquefied, as determined by comparing the liquefaction ejecta to the auger tailings. At the sites tested that did not liquefy, the augered holes were bored to the top of the potentially liquefiable layer (i.e., sand layer below the ground water table), if such a layer was found. The augered holes minimized rod friction and allowed collection of samples of the liquefiable soil. Experience has shown that the DCP can be used effectively in augered holes to depths up to 4.6 to 6.1 m.

The DCP tests consists of counting the number of drops of the 6.8 kg mass that is required to advance the cone ~4.5 cm (1.75 inches), with the number of drops, or blow count, referred to as the DCP N-value or N_{DCPT}. N_{DCPT} is approximately equal to the Standard Penetration Test (SPT) blow count up to an N-value of about 10 (Sowers and Hedges, 1966; Green et al., 2011a). However, beyond an N-value of 10, the relationship becomes non-linear. Figure 4-25a shows the relationship between SPT and DCP N-values that was used in this study, which is a slightly

modified version of the one proposed by Sowers and Hedges (1966). The modifications to Sowers and Hedges (1966) relationship are specific to the soils in the Canterbury region and are based on comparing the N_{DCPT} values to SPT N-values, Cone Penetration Test (CPT) tip resistance, and shear wave velocity measurements made near the DCP test sites.

Figure 4-24. DCP test being performed adjacent to a house in Bexley after the M_w7.1, 4 September 2010 Darfield earthquake. Brady Cox is working the hammer. (13 Sept 2010, -43.51837°, 172.72205°)

Following the procedure outlined in Olson et al. (2011), the SPT equivalent N-values ($N_{SPTequiv}$) values were normalized for effective overburden stress and hammer energy using the following relationship:

$$N_{1,60-SPT\,equiv} \approx N_{SPT\,equiv}(N_{DCPT}) \cdot \left(\frac{P_a}{\sigma'_{vo}}\right)^{0.5} \frac{ER}{60\%} \quad (1)$$

where $N_{SPT\ equiv}(N_{DCPT})$ is the functional relationship between N_{SPT} and N_{DCPT} shown in Figure 4-25a, P_a is atmospheric pressure (i.e., 101.3 kPa), σ'_{vo} is initial vertical effective stress (in the same units as P_a), and ER is energy ratio. This relationship uses the effective stress and hammer energy normalization schemes outlined in Youd et al. (2001).

Although the energy ratio for the system was not measured, the DCP hammer is similar to the donut hammer used for the SPT. Skempton (1986) and Seed et al. (1984) suggested that the energy ratio for an SPT donut hammer system ranges from about 30 to 60%. However, because the DCP system does not have pulleys, a cathead, etc., we anticipate that the energy ratio for the DCP is likely to be near the upper end of this range. Therefore, we assumed an ER = 60% for our calculations. In addition to the effective stress and hammer energy corrections, the $N_{SPT\ equiv}$ values were also corrected for fines content following the procedure proposed in Youd et al. (2001). Figure 4-25b shows a plot of N_{DCPT} and $N_{1,60cs\text{-}SPTequiv}$ for a test site in the eastern Christchurch neighborhood of Bexley, which experienced severe liquefaction during both the Darfield and Christchurch earthquakes.

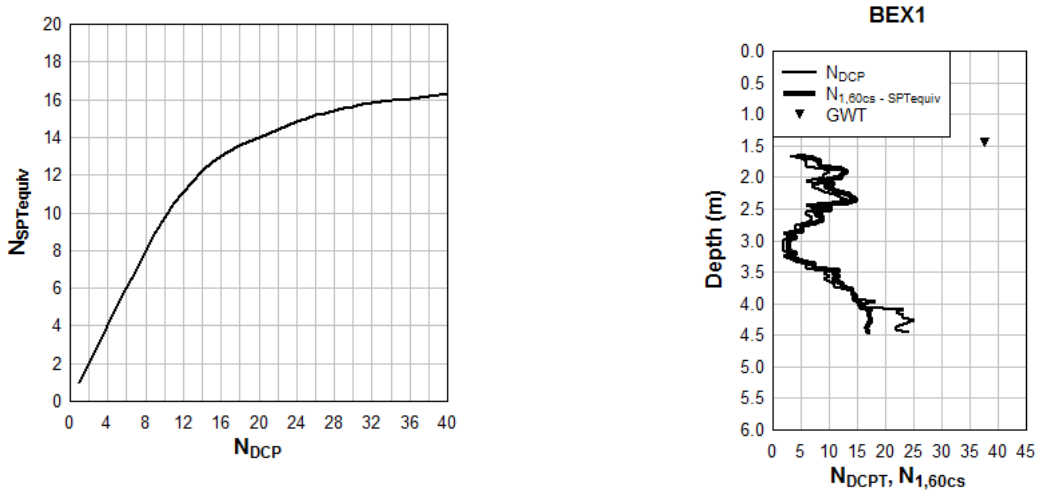

(a) (b)

Figure 4-25. (a) Relationship between DCP test and SPT N-values; and (b) comparison of N_{DCPT} and the equivalent $N_{1,60cs}$ ($N_{1,60cs\text{-}SPTequiv}$) for a test site in Bexley.

In total, 30 DCP tests were performed across Christchurch and its environs after the Darfield and Christchurch earthquakes. Figure 4-26 shows the locations of these test sites. In addition to the Darfield and Christchurch earthquakes, the DCP has been used on several other recent post-earthquake investigations to evaluate deposits that liquefied (e.g., the M_w6.3, 2008 Olfus, Iceland earthquake, the M_w7.0, 2010 Haiti earthquake, the M_w8.8, 2010 Maule, Chile earthquake, and the M_w5.8, 2011 Central Virginia, USA earthquake).

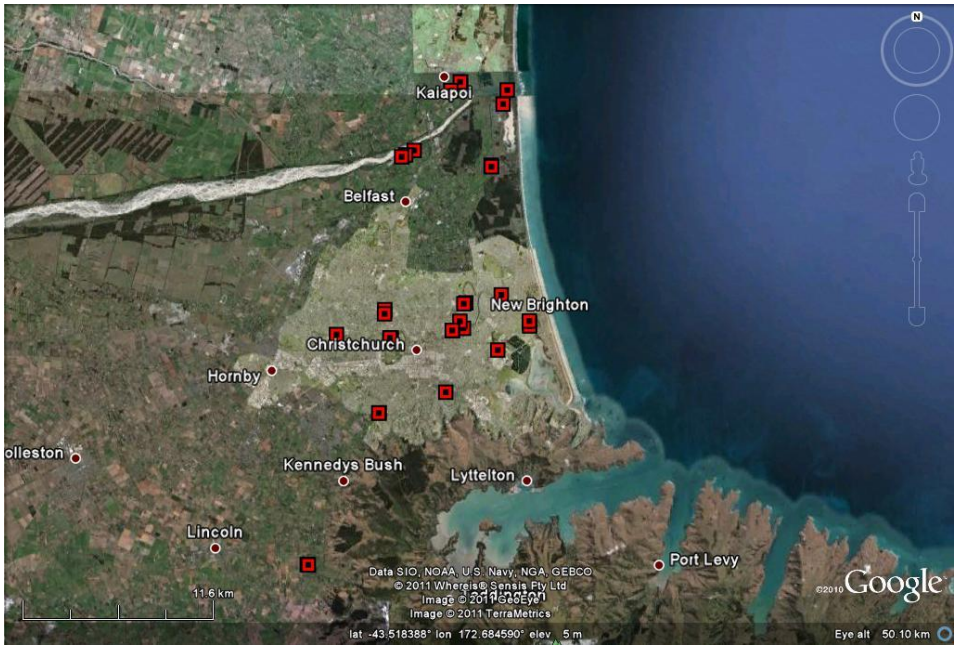

Figure 4-26. Locations of DCP test sites performed after either the Darfield or Christchurch earthquakes.

Spectral Analysis of Surface Waves (SASW)

The Spectral Analysis of Surface Waves (SASW) method is used to determine the shear wave velocity (V_S) profile at sites tested. The SASW method is widely accepted and has been used to characterize the subsurface shear stiffness of soil and rock sites for the past 20-plus years (e.g., Nazarian and Stokoe, 1984; Stokoe et al., 1994; 2003; 2004; Cox and Wood, 2010; Cox and Wood, 2011; Wong et al., 2011). In particular, the SASW method has often been applied in geotechnical earthquake engineering to characterize materials for near-surface site response analyses (e.g., Rosenblad et al., 2001; Wong and Silva, 2006) and soil liquefaction analyses (e.g., Andrus and Stokoe 2001). The SASW test is a non-intrusive, active source seismic method that utilizes the dispersive nature of Rayleigh-type surface waves propagating through a layered material to infer the subsurface V_S profile of a site.

The SASW field measurements in this study were made using three 4.5 Hz geophones, a 'pocket-portable' dynamic signal analyzer, and a sledge hammer. Figure 4-27 shows the test setup at a site in South Kaiapoi. The geophones were model GSC-11D's manufactured by Geo Space Technologies, while the analyzer was a Quattro system manufactured by Data Physics Corporation. The Quattro is a USB-powered, 4-input channel, 2-output channel dynamic signal analyzer with 205 kHz simultaneous sampling rate, 24 bit ADC, 110 dB dynamic range, and 100 dB anti-alias filters. It is controlled with a flexible, windows-based software package (Data Physics Signal Calc) that has measurement capabilities in both the time and frequency domains. The compact, highly portable nature of this setup is ideal for earthquake reconnaissance efforts

where shallow V_S profiles are desired. At most locations, receiver spacings of approximately 0.61, 1.22, 2.44, 4.88, 6.10, and 12.20 m were used to collect surface wave data. These tests took less than 45 minutes per location and typically enabled V_S profiles to be generated down to 6.1-9.1 m below the surface. In total, 36 SASW tests were performed across Christchurch and its environs after the Darfield and Christchurch earthquakes. Figure 4-28 shows the locations of the SASW test sites.

Figure 4-27. SASW setup at a site in South Kaiapoi. Liam Wotherspoon working the hammer. (12 Sept 2010; -43.39001°; 172.66264°)

Spectral analysis was used to separate the measured surface waves by frequency and wavelength to determine the experimental ("field") dispersion curve for the sites via phase unwrapping. An effective/superposed-mode inversion that takes into account ground motions induced by fundamental and higher-mode surface waves as well as body waves (i.e., a full wavefield

solution) was then used to match theoretically the field dispersion curve with a one-dimensional (1D) layered system of varying layer stiffnesses and thicknesses (Roesset et al., 1991; Joh, 1996). The 1D V_S profile that generated a dispersion curve that best matched the field dispersion curve was selected as the site profile. Per Youd et al. (2001), the V_S profiles were then normalized for effective overburden stress using the following relationship:

$$V_{s1} = V_S \left(\frac{P_a}{\sigma'_{vo}} \right)^{0.25} \tag{2}$$

where V_{S1} is the shear wave velocity normalized to 1 atm effective stress, P_a is atmospheric pressure (i.e., 101.3 kPa), and σ'_{vo} is initial vertical effective stress (in the same units as P_a). Figure 4-29 shows a plot of V_S and V_{S1} for a test site in the eastern Christchurch neighborhood of Bexley, which experienced severe liquefaction during both the Darfield and Christchurch earthquakes. Also plotted in this figure is the empirically determined upper-bound V_{S1} for liquefiable soils (i.e., soils having $V_{S1} > V^*_{S1}$ will not liquefy regardless of the intensity of shaking imposed on them).

Figure 4-28. Locations of SASW test sites performed after either the Darfield or Christchurch earthquakes.

Estimation of PGAs at DCP and SASW Test Sites

As discussed in the next section, the in-situ test data described above correlates to the ability of the soil to resist liquefaction (i.e., capacity). However, to evaluate liquefaction potential, both the soil's ability to resist liquefaction and the demand imposed on the soil by the earthquake needs to

be known. For the approach used herein to evaluate liquefaction potential (i.e., stress-based simplified procedure), the amplitude of cyclic loading correlates to the PGA at the ground surface and the duration correlates to earthquake magnitude. Accordingly, the PGAs at the sites where DCP and SASW tests were performed needed to be estimated for both the Darfield and the Christchurch earthquakes. As outlined below, the PGAs recorded at the strong motion stations (refer to Chapter 2) were used to compute the conditional PGA distribution at the test sites.

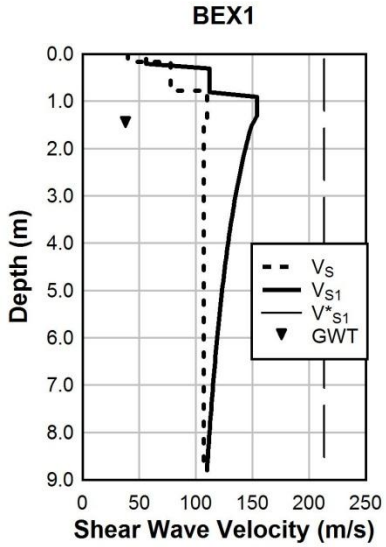

Figure 4-29. Measured V_S and corrected V_{S1} profiles for a test site in Bexley. Also shown is the theoretical limiting upper-bound value of V_{S1} for liquefaction triggering (V^*_{S1}) for soil having FC = 9%.

The ground motion at a strong motion station *i* can be expressed as:

$$\ln(PGA_i) = \ln \overline{PGA_i}(Site, Rup) + \eta + \varepsilon_i \quad (3)$$

where $\ln(PGA_i)$ is the natural logarithm of the observed PGA at station i; $\ln \overline{PGA_i}(Site, Rup)$ is the predicted median natural logarithm of PGA at the same station by an empirical ground motion prediction equation (GMPE), which is a function of the site and earthquake rupture; η is the inter-event residual; and ε_i is the intra-event residual. Based on Equation (3), empirical GMPE's provide the distribution (unconditional) of ground motion shaking as:

$$\ln(PGA_i) \sim N\left(\ln \overline{PGA_i}, \sigma_\eta^2 + \sigma_\varepsilon^2\right) \quad (4)$$

where $X \sim N(\mu_X, \sigma_X^2)$ is short-hand notation for X having a normal distribution with mean μ_X and variance σ_X^2.

By definition, all recorded PGAs from a single earthquake have the same inter-event residual, η. On the other hand, the intra-event residual, ε_i, varies from site-to-site, but is correlated spatially due to similarities of path and site effects among various locations. Accordingly, use can be made of recorded PGAs at strong motion stations (e.g., Chapter 2) to compute a conditional distribution of PGAs at the DCP and SASW test sites.

Firstly, the empirical GMPE proposed by Bradley (2010) was used to compute the unconditional distribution of PGAs at the strong motion stations. A mixed-effects regression was then used to determine the inter-event residual, η, and the intra-event residuals, ε_i's, for each strong motion station (Abrahamson and Youngs, 1992; Pinheiro et al., 2008).

Secondly, the covariance matrix of intra-event residuals was computed by accounting for the spatial correlation between all of the strong motion stations and a test site of interest. The joint distribution of intra-event residuals at a test site of interest and the strong motion stations is given as:

$$\begin{bmatrix} \epsilon^{site} \\ \boldsymbol{\epsilon^{SMstation}} \end{bmatrix} = N\left(\begin{bmatrix} 0 \\ \mathbf{0} \end{bmatrix}, \begin{bmatrix} \sigma^2_{\epsilon_{site}} & \boldsymbol{\Sigma}_{12} \\ \boldsymbol{\Sigma}_{21} & \boldsymbol{\Sigma}_{22} \end{bmatrix}\right) \tag{5}$$

where $X \sim N(\mu_X,\Sigma)$ is short-hand notation for X having a multivariate normal distribution with mean μ_X and covariance matrix Σ (i.e., as before, but in vector form); and $\sigma^2_{\varepsilon\text{-}site}$ is the variances in the intra-event residual at the site of interest. In Equation (5), the covariance matrix has been expressed in a partitioned fashion to elucidate the subsequent computation of the conditional distribution of ε^{site}. The individual elements of the covariance matrix were computed from:

$$\boldsymbol{\Sigma}(i,j) = \rho_{i,j}\sigma_{\epsilon_i}\sigma_{\epsilon_j} \tag{6}$$

where $\rho_{i,j}$ is the spatial correlation of intra-event residuals between the two locations i and j; and $\sigma_{\varepsilon i}$ and $\sigma_{\varepsilon j}$ are the standard deviations of the intra-event residual at locations i and j. Based on the joint distribution of intra-event residuals given by Equation (5), the conditional distribution of ε^{site} was computed from (Johnson et al., 2007):

$$\begin{aligned} \left[\epsilon^{site}\middle|\boldsymbol{\epsilon^{SMstation}}\right] &= N\left(\boldsymbol{\Sigma}_{12}\cdot\boldsymbol{\Sigma}_{22}^{-1}\cdot\boldsymbol{\epsilon^{SMstation}}, \sigma^2_{\epsilon_{site}} - \boldsymbol{\Sigma}_{12}\cdot\boldsymbol{\Sigma}_{22}^{-1}\cdot\boldsymbol{\Sigma}_{21}\right) \\ &= N\left(\mu_{\epsilon^{site}|\boldsymbol{\epsilon^{SMstation}}}, \sigma^2_{\epsilon^{site}|\boldsymbol{\epsilon^{SMstation}}}\right) \end{aligned} \tag{7}$$

Using the conditional distribution of the intra-event residual at a test site of interest given by Equation (7) and substituting into Equation (4), the conditional distribution of the PGA_i was computed from:

$$[lnPGA_{site}|ln\boldsymbol{PGA_{SMstation}}] = N\left(ln\overline{PGA_{site}} + \eta + \mu_{\epsilon^{site}|\boldsymbol{\epsilon^{SMstation}}}, \sigma^2_{\epsilon^{site}|\boldsymbol{\epsilon^{SMstation}}}\right) \tag{8}$$

It should be noted that in cases where the test site of interest was located far from any strong motion station the conditional distribution was similar to the unconditional distribution, and for test sites of interest located very close to a strong motion station the conditional distribution approached the value observed at the strong motion station.

To estimate the PGAs at the DCP and SASW test sites, the unconditional PGAs were estimated using the empirical GMPE proposed by Bradley (2010) and the conditional PGAs were estimated following the approach outlined above wherein the spatial correlation model of Goda and Hong (2008) was used.

Liquefaction Evaluation

Using the PGAs determined as described above, the cyclic stress ratios (CSRs) at the DCP test sites, for both the Darfield and Christchurch earthquakes, were calculated following the methodology outlined in Youd et al. (2001). The average of the recommended range of magnitude scaling factors (MSFs) proposed in Youd et al. (2001) was used to compute $CSR_{M7.5}$ at the sites.

As outlined previously, equivalent SPT $N_{1,60}$ values were determined from the N_{DCPT} values using Equation (1). These values were then corrected for fines content (FC) using the procedure proposed in Youd et al. (2001). For many of the sites, samples of the liquefiable soil were collected and analyzed in the laboratory to determine the FC. However, for sites where no samples were collected, FC = 12% was assumed, which is representative of the approximate fines content of soils at the sites sampled. Once the $N_{1,60cs\text{-}SPTequiv}$ were determined, the correlation proposed by Youd et al. (2001) was used to estimate the cyclic resistance ratio for a M_w7.5 event (i.e., $CRR_{M7.5}$). Comparisons of the computed $CSR_{M7.5}$ for both the Darfield and Christchurch earthquakes and $CRR_{M7.5}$ for a test site in the eastern Christchurch suburb of Bexley are shown in Figure 4-30a. As shown in this figure, liquefaction is predicted to have occurred during both earthquakes (i.e., $CSR_{M7.5} > CRR_{M7.5}$). However, the factor of safety against liquefaction (FS) is lower for the Christchurch earthquake than the Darfield earthquake; where $FS = CRR_{M7.5}/CSR_{M7.5}$. The lower factor of safety indicates increased severity of liquefaction. These predictions are consistent with field observations in Bexley made shortly after the two earthquakes (i.e., liquefaction occurred during both earthquakes, but was more severe during the Christchurch earthquake).

To compare the predicted versus observed liquefaction at all the DCP test sites, each of the DCP logs was analyzed for quality and critical depths for liquefaction/thickness of the critical layers were selected. Logs where refusal was met within ~0.3 to 0.5 m of the start of the test were removed from the database, where refusal was taken as $N_{DCPT} > \sim 35$ for more than two 4.5 cm drives. The reason for this is that too little of the profile was tested in these cases to make a meaningful interpretation. The thicknesses of the critical layers were selected based on how liquefaction manifested at the ground surface. In general, the selected critical layer thickness was

thinnest for cases of lateral spreading with no ejecta, intermediate for lateral spreading with ejecta, and thickest for large sand boils with no associated lateral spreading. For example, the profile shown in Figure 4-30a laterally spread (see Figure 4-24) and there was a significant amount of ejecta that vented to the ground surface nearby. Using this information, and trends in the N_{DCPT}, shown in Figure 4-25b, the selected critical layer was ~2 m thick, as indicated in Figure 4-30a. Once the critical layers were determined for each test site, the $N_{1,60cs\text{-}SPTequiv}$ values, $CSR_{M7.5}$, and $CRR_{M7.5}$ were averaged over these depths. The results were plotted along with Youd et al. (2001) SPT $CRR_{M7.5}$ curve in Figure 4-31a.

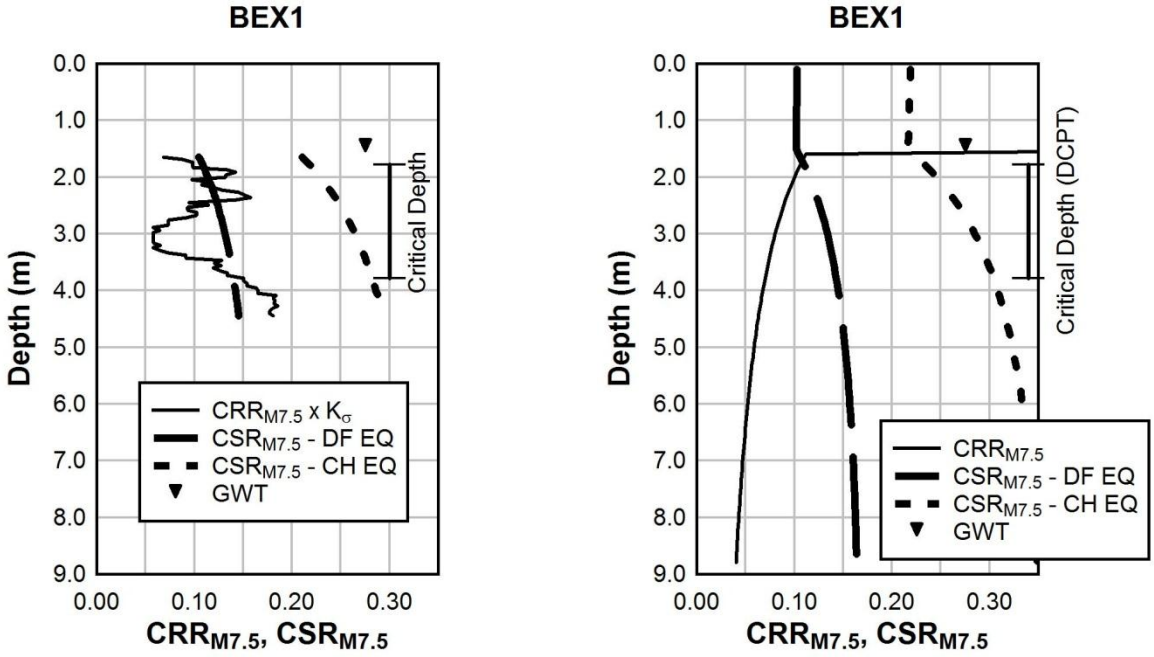

Figure 4-30. Comparison of $CSR_{M7.5}$ for the Darfield and Christchurch earthquakes with $CRR_{M7.5}$ for a site in Bexley (FC = 9%): (a) profiles for DCP test; and (b) profiles for SASW test.

A similar procedure as that outlined above was used to compute the $CSR_{M7.5}$ for the SASW test sites. However, the MSF proposed by Andrus and Stokoe (2000) was used instead of the average of the recommended range proposed by Youd et al. (2001). The reason for using slightly different MSFs was to be consistent with how the respective cyclic resistance ratio curves were developed from the observational data. Using the computed V_{S1}, the $CRR_{M7.5}$ for the test site profiles were calculated following the Andrus and Stokoe (2000) procedure; this procedure is also outlined in Youd et al. (2001). Comparisons of the computed $CSR_{M7.5}$ for both the Darfield and Christchurch earthquakes and $CRR_{M7.5}$ for a test site in the eastern Christchurch suburb of Bexley are shown in Figure 4-30b. Consistent with the DCP test results, liquefaction is predicted to occur at this site during both the Darfield and Christchurch earthquakes, with the liquefaction

predicted to be more severe during the Christchurch earthquake. Again, these predictions are in line with the post-earthquake observations.

Using the same critical layers as selected for DCP test liquefaction evaluations, V_{S1}, $CSR_{M7.5}$, and $CRR_{M7.5}$ were averaged over the critical depths for each test site profile. The results were plotted along with Andrus and Stokoe (2000) $CRR_{M7.5}$ curves in Figure 4-31b.

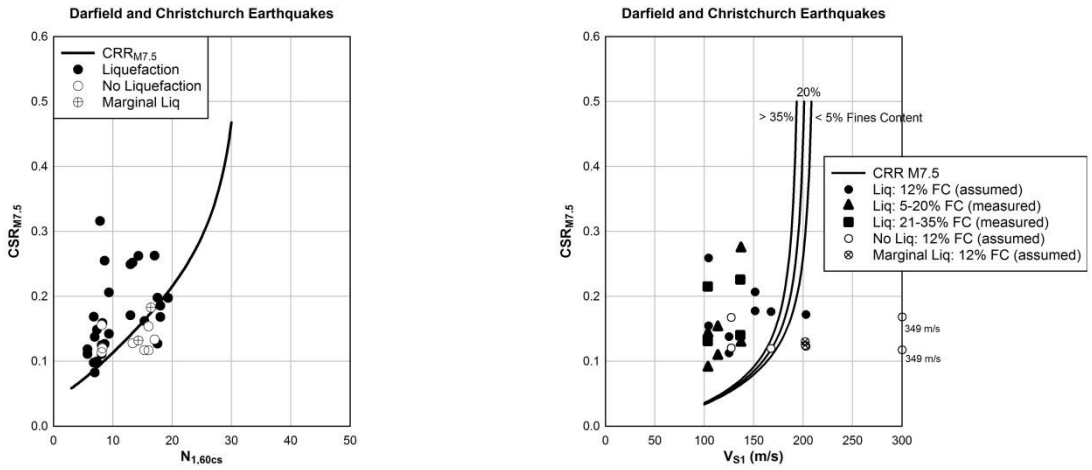

(a) (b)

Figure 4-31. Comparison of predicted versus observed liquefaction: (a) DCPT test; and (b) SASW test.

As shown in Figure 4-31, the liquefaction predictions made using both the DCP and SASW test data reasonably match field observations. This is particularly significant for the DCP data because a correlation was first required to convert the measured N_{DCPT} to SPT N-values (shown in Figure 4-25a), and undoubtedly, this correlation is inherently uncertain. Also, the DCP was only able to test down to a depth of ~6 m at a maximum and usually less than about 4.5 m. Below this depth, N_{DCPT} became large because of the presence of a dense layer and/or because of the increase in effective confining stress. Because the DCP is manually operated, performing tests beyond ~5 m depths becomes very laborious even in relatively loose sand deposits. The SASW test was able to test to deeper depths that the DCP, but was still limited to depths of ~ 6 to 9 m with the sledge hammer source. These depth limits are true short-comings of both tests because at a few DCP and SASW test sites, available cone penetration test (CPT) soundings indicated the presence of potentially liquefiable layers deeper in the profiles. As a result, our selected critical layer may only be one of multiple critical layers in the profile and may not be the most critical.

Also from Figure 4-31, it can be noted that most of the DCP and SASW tests were performed at sites that liquefied, with a paucity of data from sites that did not liquefy. The reason for this is

the manifestation of liquefaction at the ground surface is a definite indication that liquefiable soils are present. Several no-liquefaction sites were investigated, especially ones adjacent to sites that liquefied. However, in the majority of these cases we were not able to find a sandy stratum below the ground water table in the upper ~5 m of these sites using the hand-auger. As a result, DCP tests were not performed at these sites, and the sites were not included in the DCP database.

References

Abrahamson, N.A. and R.R. Youngs (1992). A Stable Algorithm for Regression Analyses Using the Random Effects Model, Bulletin of the Seismological Society of America, **82**(1), 505-510.

Andrus, R.D., and K.H. Stokoe II (2000). Liquefaction resistance of soils from shear wave velocity, *ASCE Journal of Geotechnical and Geoenvironmental Engineering*, **126**(11), 1015-1025.

Archives New Zealand (2011). *Black Map of Christchurch, March 1850.* http://archives.govt.nz/gallery/v/Online+Regional+Exhibitions/Chregionalofficegallery/sss/Black+Map+of+Christchurch/. Last accessed July 18, 2011.

Bradley, B.A. (2010). NZ-Specific Pseudo-Spectral Acceleration Ground Motion Prediction Equations Based on Foreign Models, Department of Civil and Natural Resources Engineering, University of Canterbury, Christchurch, New Zealand, 324pp.

Bradley, B.A. and Cubrinovski, M. (2011). Near-source strong ground motions observed in the 22 February 2011 Christchurch earthquake, *Seismological Research Letters*, **82**(6), 853-865.

Brown, L.J. and J.H. Weeber (1992). *Geology of the Christchurch Urban Area*. Institute of Geological and Nuclear Sciences. Lower Hutt, New Zealand: GNS Geoscience

Cox, B.R. and C.M. Wood (2010). A Comparison of Linear-Array Surface Wave Methods at a Soft Soil Site in the Mississippi Embayment, *GeoFlorida 2010: Advances in Analysis, Modeling and Design* (Fratta et al., eds.), ASCE GSP 199.

Cox, B.R. and C.M. Wood (2011). Surface Wave Benchmarking Exercise: Methodologies, Results and Uncertainties, *GeoRisk 2011: Geotechnical Risk Assessment and Management* (C.H. Juang et al., eds), ASCE GSP 224.

Cubrinovski, M., J.D. Bray, M. Taylor, S. Giorgini, B. Bradley, L. Wotherspoon, and J. Zupan (2011a). Soil Liquefaction Effects in the Central Business District during the February 2011 Christchurch Earthquake, Seismological Research Letters, **82**(6), 893-904.

Cubrinovski, M., Bradley, B. Wotherspoon, L., Green, R.A., Bray, J., Wood, C., Pender, M., Allen, J., Bradshaw, A., Rix, G., Taylor, M., Robinson, K., Henderson, D., Giorgini, S., Ma, K.,

Winkley, A., and Zupan, J. (2011b). Geotechnical Aspects of the 22 February 2011 Christchurch Earthquake, *Bulletin of the New Zealand Society for Earthquake Engineering*, (in press).

Cubrinovski, M. and McCahon, I. (2011). Foundations on Deep Alluvial Soils, University of Canterbury, Christchurch, 40pp.

Cubrinovski, M., R. Green, J. Allen, S. Ashford, E. Bowman, B. Bradley, B. Cox, T. Hutchinson, E. Kavazanjian, R. Orense, M. Pender, M. Quigley, and L. Wotherspoon (2010). Geotechnical Reconnaissance of the 2010 Darfield (Canterbury) Earthquake. *Bulletin of the New Zealand Society for Earthquake Engineering*, **43**(4), 243-320.

Goda, K. and H.P. Hong (2008). Spatial Correlation of Peak Ground Motions and Response Spectra, *Bulletin of the Seismological Society of America*, **98**(1), 354-465.

Green, R.A., Cubrinovski, M., Wotherspoon, L., Allen, J., Bradley, B., Bradshaw, A., Bray, J., DePascale, G., Orense, R., O'Rourke, T., Pender, M., Rix, G., Wells, D., Wood, C., Henderson, D., Hogan, L., Kailey, P., Robinson, K., Taylor, M., and Winkley, A. (2012). "Geotechnical Effects of the M_W6.1 2011 Christchurch, New Zealand Earthquake", *Proc. GeoCongress 2012: State of the Art and Practice in Geotechnical Engineering*, Oakland Marriott City Center, Oakland, CA, 25-29 March. (*in press*)

Green, R.A., S.M. Olson, B.R. Cox, G.J. Rix, E. Rathje, J. Bachhuber, J. French, S. Lasley, and N. Martin (2011a). Geotechnical Aspects of Failures at Port-au-Prince Seaport During the 12 January 2010 Haiti Earthquake, *Earthquake Spectra*, **27**(S1), S43-S65.

Green, R.A., Wood, C., Cox, B., Cubrinovski, M., Wotherspoon, L., Bradley, B., Algie, T., Allen, J., Bradshaw, A., and Rix, G. (2011b). "Use of DCP and SASW Tests to Evaluate Liquefaction Potential: Predictions vs. Observations During the Recent New Zealand Earthquakes", *Seismological Research Letters*, **82**(6), 861-872.

Joh, S.H. (1996). Advances in interpretation and analysis techniques for spectral-analysis-of-surface-waves (SASW) measurements. Ph.D. Dissertation, Dept. of Civil, Architectural, and Environmental Engineering, University of Texas, Austin, TX, 240 p.

Johnson, R.A. and D.W. Wichern (2007). Applied Multivariate Statistical Analysis, Prentice-Hall, Upper Saddle River, NJ.

Nazarian, S. and K.H. Stokoe II. (1984). In situ shear wave velocities from spectral analysis of surface wave tests. *Proc. Eighth World Conference on Earthquake Engineering*, San Francisco, California, 31-38.

New Zealand Government (2011). http://www.beehive.govt.nz/release/govt-outlines-next-steps-people-canterbury. Last accessed July 18, 2011.

Olson, S.M., R.A. Green, S. Lasley, N. Martin, B.R. Cox, E, Rathje, J. Bachhuber, and J. French (2011). Documenting Liquefaction and Lateral Spreading Triggered by the 12 January 2010 Haiti Earthquake, *Earthquake Spectra*, **27**(S1), S93-S116.

Pinheiro, J., D.M. Bates, S. DebRoy, D. Sarkar, and the R Core Team (2008). nlme: linear and nonlinear mixed effects models, *R package version 3.1*, 89pp.

Roesset J.M., D.W. Chang, and K.H. Stokoe II (1991). Comparison of 2-D and 3-D models for analysis of surface wave tests, *Proc. 5th Int. Conf. on Soil Dynamic and Earthquake Engineering*, Vol. 1, 111-126.

Rosenblad, B.L., K.H. Stokoe II, E.M. Rathje, and M.B. Darendeli (2001). Characterization of strong motion stations shaken by the Kocaeli and Duzce earthquake in Turkey: Geotechnical Engineering Report GR01-1, Geotechnical Engineering Center, University of Texas at Austin.

Seed, H.B., K. Tokimatsu, L.F. Harder, and R. Chung (1984). The Influence of SPT Procedures on Soil Liquefaction Resistance Evaluations, Report No. UCB\EERC-84/15, Earthquake Engineering Research Center, Univ. California, Berkeley, CA.

Skempton, A.W. (1986). Standard Penetration Test Procedures and the Effects in Sands of Overburden Pressure, Relative Density, Particle Size, Aging and Overconsolidation, *Geotechnique*, **36**(3), 425-447.

Sowers, G.F. and C.S. Hedges (1966) Dynamic cone for shallow in-situ penetration testing, vane shear and cone penetration resistance testing of in-situ soils. *ASTM STP 399, American Society of Testing Materials*, Philadelphia, PA, 29-37.

Stokoe II, K.H., S.G. Wright, J.A. Bay, and J.M. Roesset (1994). Characterization of geotechnical sites by SASW method, *Proc. 13th International Conference on Soil Mechanics and Foundation Engineering*, **22** (9-12), 923-930.

Stokoe II, K.H., S.H. Joh, and R.D. Woods (2004). Some contributions of *in situ* geophysical measurements to solving geotechnical engineering problems, *Proc. International Site Characterization ISC'2 Porto*, Portugal.

Stokoe II, K.H., B.L. Rosenblad, J.A. Bay, B. Redpath, J.G. Diehl., R. Steller, I.G. Wong, P.A. Thomas, and M. Luebbers (2003). Comparison of V_S profiles from three seismic methods at Yucca Mountain, *Proc. Soil and Rock America 2003* (P.J. Culligan et al., eds), Verlag Glückauf GMBH, 1, 299-306.

Wong, I. and W. Silva (2006). The importance of in-situ shear-wave velocity measurements in developing urban and regional earthquake hazard maps, *Proc. 19th Annual Symposium on the Application of Geophysics to Engineering and Environmental Problems*, 1304-1315.

Wong, I., K.H. Stokoe II, B.R. Cox, Y.-C. Lin, and F.-Y. Menq (2011). Shear-Wave Velocity Profiling of Strong Motion Sites that Recorded the 2001 Nisqually, Washington Earthquake, *Earthquake Spectra*, **27**(1), 183-212.

Wotherspoon, L.M., M.J. Pender, and R.P. Orense (2011). Relationship between observed liquefaction at Kaiapoi following the 2010 Darfield earthquake and former channels of the Waimakariri River, *Engineering Geology*, (in press).

Youd, T.L., I.M. Idriss, R.D. Andrus, I. Arango, G. Castro, J.T Christian,. R. Dobry, W.D.L. Finn, L.F. Harder, M.E. Hynes, K. Ishihara, J.P. Koester, S.S.C. Liao, W.F. Marcuson III, G.R. Martin, J.K. Mitchell, Y. Moriwaki, M.S. Power, P.K. Robertson, R.B. Seed, and K.H. Stokoe II (2001). Liquefaction resistance of soils: summary report from the 1996 NCEER and 1998 NCEER/NSF workshops on evaluation of liquefaction resistance of soils. *Journal of Geotechnical and Geoenvironmental Engineering, ASCE*, **127**(10), 817-833.